AERODYNAMICS AND ACOUSTICS OF BLADE-VORTEX INTERACTION USING AN INDEPENDENTLY GENERATED VORTEX

C. Kitaplioglu* and F.X. Caradonna+
NASA Ames Research Center
Moffett Field, California

Abstract

This paper presents results from an experimental study of rotor blade-vortex interaction (BVI) aerodynamics and acoustics. The experiment utilized an externally generated vortex interacting with a two-bladed rotor operating at zero thrust to minimize the influence of the rotor's own wake. The rotor blades were instrumented with a total of 60 absolute pressure transducers at three spanwise and ten chordwise stations on both the upper and lower surfaces. Acoustic data were obtained with fixed near-field microphones as well as a movable array of far-field microphones. The test was carried out in the acoustically treated test section of the NASA Ames 80- by 120-Foot Wind Tunnel. Several crucial parameters of BVI, such as vortex-rotor separation distance, vortex strength, and vortex sense (swirl direction), as well as rotor tip Mach number and advance ratio were varied. Simultaneous measurements were obtained of blade surface pressure distributions, near-field acoustics, and far-field acoustics during the vortex-blade encounters. Vortex-blade proximity and rotor tip Mach number were found to be the most important determining parameters of BVI noise.

Nomenclature

c	blade chord
R	rotor radius
α_v	vortex generator angle of attack
z_v	vortex location relative to rotor plane
x, y, z	coordinate system centered on the rotor hub
ψ	azimuth angle measured positive in direction of rotation; ψ=0 is downstream
ϕ	elevation angle measured positive down from rotor plane
μ	rotor advance ratio
M_{tip}	hover tip Mach number
$C_p = (p - p_s)/0.5*\rho*V_\infty^2$	pressure coefficient
ρ	density
V_∞	tunnel free stream velocity
p	pressure
p_s	static pressure
$L_p = 20 \log_{10}(p/p_{ref})$	Sound Pressure Level (dB)
p_{ref}	reference pressure (2×10^{-5} Pascals, unless otherwise noted)

---

* Aerospace Engineer, NASA Ames Research Center
+ Staff Scientist, U.S. Army ATCOM Aeroflightdynamics Directorate

Presented at the American Helicopter Society Aeromechanics Specialists Conference, San Francisco, California, January 19-21, 1994.

Introduction

The interaction of a rotor with one or more of its tip-vortices can occur in many forms and is a topic of considerable interest. Such interactions are a primary source of rotor vibratory loading. When the rotor blade and the tip-vortex are very close and nearly parallel to each other the interaction is particularly strong (though of short duration) and is a major source of rotorcraft noise. This type of interaction is usually referred to as a parallel "BVI" (Blade-Vortex Interaction) and is the subject of this experimental investigation.

A large number of aerodynamic and acoustic computational codes (Refs. 1-5), embodying a wide range of physical models of BVI, have been developed. The aerodynamic models range from two-dimensional, ideal-flow, "vortex-cloud" methods employing conformal mapping solutions to full 3-D, compressible Euler/Navier-Stokes CFD methods - with the middle-ground being held by 3-D full-potential CFD methods. Acoustic prediction methods are of two types; the acoustic analogy methods and the more recent Kirchoff methods. CFD is also used for acoustics but cannot practically be extended to the great distances that acoustics is ultimately concerned with. Nevertheless, CFD has great potential for providing input for Kirchoff methods. The choice between these methods is dependent on the extent to which flow-field non-linearity dominates the solution. Therefore the near-field aerodynamics is of critical importance both for determining the essential physics and the type of acoustic method that must be used. It is crucially important that we develop combined aeroacoustic computational methods in which we have high confidence. Such confidence requires validation using the simplest possible tests. Until the present, however, all BVI aeroacoustic tests have involved the use of full rotor models operating at typical flight conditions. The complexities of typical rotor flows (with wake geometries whose strength and locations with respect to the blade are difficult to determine) are considerable. We have taken a different approach by performing an experiment which, rather than operating a rotor under typical flight conditions generating BVI, creates a situation that closely resembles the simplified geometry found in the most basic CFD codes. In effect, rather than refining the model to account for real world complexities, we have attempted to refine the experiment to reflect the simplest possible computational model of BVI. If the codes cannot do a good job of correlating with a simplified experiment, there is little reason to expect good correlation with real flight data with all of its complications.

This paper describes a wind tunnel experiment to investigate the fundamentals of BVI aeroacoustics and presents some representative blade pressure and far-field acoustic data.

Description of Experiment

Background

The objective of the test was to experimentally simulate the aerodynamics and acoustics of parallel (2-D), unsteady BVI. The main point of the test was to set up a situation that matched, as closely as possible, the simplified model of a rotor blade undergoing an unsteady, parallel interaction with a vortex. Figure 1, taken from Ref. 1, illustrates this simple 2-D BVI model. To provide independent control of the interaction parameters, the vortex was generated separately by a wing tip, placed upstream of the rotor and set at an angle of attack. The rotor was operated at zero thrust to minimize the influence of the rotor's own wake/tip-vortex system. The relative positions of the rotor and wing ensure parallelism of the interaction. Figures 2 and 3 illustrate the experimental arrangement. Two similar experiments were previously performed by Caradonna (Refs. 6-8); however, that work focused on the aerodynamic aspects of the problem and did not include acoustic measurements because the wind tunnel utilized had acoustically reflective walls. The present experiment extends that work to include acoustic studies.

This is a practical way to approximate a 2-D, unsteady interaction, although the complication of rotational and 3-D tip effects is introduced. Since the latter are important for rotors, this is not felt to be a serious shortcoming of the experiment. Codes specifically applicable to rotors will be expected to account for these effects. Alternative methods (Refs. 9-10) of generating parallel, unsteady interactions are not as amenable to control nor as repeatable as the present method. For example, to generate a parallel interaction using a fixed blade requires generation of either a periodic or an impulsive vortex. Both of these, although unsteady in nature, would be difficult to control and, most likely, have an unnecessarily complex core structure. In addition, this type of an experiment would require either a small wind tunnel or a complicated arrangement of end plates to maintain two-dimensionality, a distinct disadvantage for acoustic measurements.

The major parameters expected to influence parallel, unsteady BVI are vortex strength and sense, determined by the vortex generator angle of attack (α_v), vortex-blade separation distance (z_v), rotor advance ratio (μ), and hover tip Mach number (M_{tip}). These were all independently controlled. The location of the vortex relative to

the blade was measured using a laser sheet/high speed video arrangement. The parallelism of the set up was checked with a separate synchronized strobe and video set. The blade surface pressures and the acoustic field were simultaneously measured for each specific interaction geometry. The surface pressure distribution was measured with a chordwise and spanwise array of transducers. Two sets of acoustic measurements were made. Two microphones in the near-field of the interaction provided information on the detailed evolution of the acoustic field and can serve to validate "mid-field" calculations of computational aeroacoustics and Kirchoff methods. A movable array of microphones was used to obtain a limited (due to time constraints) survey of the acoustic far-field.

Rotor and test stand

The rotor system is a small-scale (7-foot diameter), two-bladed, teetering rotor. The blades are untwisted, have a rectangular planform with NACA 0012 airfoil sections and 6-inch chord. The blade Reynolds Number was of the order of 1,000,000. The blades are constructed of carbon composite material and are not dynamically scaled. Each blade is equipped with 30 absolute pressure transducers, one blade on the upper surface, the other on the lower surface. The transducers are distributed in three spanwise sets of ten chordwise locations. Figure 4 details the transducer locations. The transducers as installed had a calibrated frequency response above 10kHz.

The rotor was mounted on the Army Rotary Wing Test Stand (RWTS) which is capable of driving the rotor up to 2300 RPM (tip Mach number of 0.75). Rotation was in the clockwise direction (when viewed from above the rotor). The long drive shaft was housed within an aerodynamic fairing covered with foam to minimize acoustic reflections. The RWTS has an internal six-component balance for measuring rotor loads-and incorporates a 256-channel slip-ring assembly for routing blade safety and pressure transducer data. The RWTS also incorporates two encoders that provide 1/rev and 1024/rev TTL signals to facilitate data acquisition. The rotor controls consisted of an RPM control plus collective and cyclic pitch actuators that accepted direct input from a control box. Shaft angle was fixed.

Vortex generator

The vortex was generated using a short rectangular wing with an 18-inch chord, a NACA 0015 airfoil, and a Reynolds Number of the order of 600,000. The generated vortex had a large core size of approximately 0.5 rotor blade chord. The wing is constructed in a two-piece telescoping arrangement to allow changes in vertical positioning of the vortex relative to the rotor blade. It has a total travel of 9 inches and can be remotely traversed. The wing incorporates internal tubing to allow introduction of smoke near the tip for flow visualization. During this experiment theatrical "fog juice" was used to make the vortex visible. The wing angle of attack, α_V, was manually set.

The vortex generator wing was mounted on an airfoil-shaped stand for positioning at the appropriate height. The stand was constructed of perforated sheet metal covered with foam to prevent acoustic reflections. The interface between the stand and wing had provision for fine adjustment of lateral position (to ensure parallel interaction at the correct azimuth position of the rotor). The entire arrangement can also be translated streamwise and laterally for future studies of oblique interactions and vortex age effects.

Tip vortex strength and structure were not measured during this test. However, detailed laser velocimetry studies of a very similar half-span wing were conducted in the Army 7- by 10-Foot Wind Tunnel by McAlister and Takahashi (Ref. 11). Although this test involved many of the same incidences as the McAlister test, it is possible that there are differences due to differences in tunnel wall effects.

Microphones

Two sets of microphones were installed for acoustic measurements. One set consisted of five microphones mounted at various heights on a remotely controlled traversing vertical strut. The traverse was mounted on the tunnel floor 10.04 feet to the side of the rotor placing the vertical mic array at any azimuth angle between 225 deg and 315 deg relative to the rotor hub. The five microphones were placed at elevation angles of 26, 32, 37, 43, and 47 deg (Fig. 5) below the rotor hub (when the strut was in line with the hub). This arrangement provided a detailed map of the acoustic far-field in the starboard quarter and below the rotor. Pre-test predictions indicated the acoustic radiation pattern to be in this direction for the test configuration.

Another set of two microphones were mounted on a short boom from the RWTS placing them just under and to the side of the interaction position. They were approximately two blade-chords from the leading edge of the blade at the 180 deg azimuth position (Fig. 6). These yielded near-field measurements of the noise field. Their purpose was to enable correlation with computational and Kirchoff "mid-field" prediction results.

Bruel & Kjaer (B&K) 1/2-inch microphones with appropriate cathode followers and power supplies were used. For the wind-on data runs, standard B&K nose cones were installed.

Wind tunnel installation

The test was performed in the NASA Ames 80- by 120-Foot Wind Tunnel. The test section has approximately six inches of acoustic treatment in the floor and ceiling and ten inches in the walls, yielding a cutoff frequency (for 90 percent absorption) of approximately 250 Hz. Although insufficient to accurately measure blade passage frequencies (60-70 Hz for this test), the treatment is adequate to measure the higher harmonics that are of most interest for BVI noise.

The RWTS/rotor system was installed on the horizontal centerline of the test section, with the rotor hub 15.65 feet above the tunnel floor. All model controls were in the tunnel control room.

The vortex generator (VG) was installed upstream of the RWTS with the trailing edge of the wing 48 inches upstream of the rotor blade tip at its 180 deg azimuth position. The height of the VG stand was such as to place the vortex for direct impact with the blade when the wing was at the mid-point of its extension limits. This allowed for placement of the vortex both above and below the blade. The VG vertical position could be remotely set from the control room. The smoke generator for flow visualization was mounted inside the vortex generator.

The microphone traverse system was installed approximately ten feet to starboard of the RWTS and aligned with the flow. From the nominal "zero" position directly to the side of the rotor hub, the microphone strut carrying the five far-field microphones could traverse upstream and downstream for distances of over ten feet; thus azimuth angles of 225 - 315 deg relative to the hub could be probed.

A long range laser, used to illuminate the vortex (seeded with smoke) and blade during the encounter to document their separation distance, was installed approximately 25 ft to the side of the RWTS. The adjustable laser optics allowed positioning the laser sheet to intersect the blade and vortex just inboard of the tip. This cross-section of the BVI event was recorded on a special high-speed, low-light video camera, mounted approximately 30 ft upstream of the RWTS. The camera shutter was slaved to the 1/rev trigger to capture the BVI event. A strobe, also slaved to the 1/rev trigger illuminated the blade from below. A standard video camera, also mounted below the rotor, verified that the vortex and blade were parallel during the encounter.

Test procedures

Prior to the start of actual testing, some preliminary runs were carried out to check the acoustic reflection characteristics of the test arrangement and to calibrate the video system for quantitative measurements of the vortex-blade separation distance. Wind-on background noise measurements were performed after the completion of the data runs.

The testing proceeded in several stages. Since the vortex generator angle of attack had to be set manually, each stage corresponded to one value of this parameter and consisted of two sets of runs. The first set was dedicated to flow visualization, while the second set was for blade pressure and acoustic data acquisition.

Flow visualization determined the vertical position of the vortex generator that would yield the required vortex-blade separation distance and ensured that the blade and the vortex were parallel during the encounter. During flow visualization, the pressure transducers were covered with tape to avoid contamination by the smoke particles. At each μ and M_{tip}, the smoke was released and the vortex generator was moved to a set of vertical positions. Adjustments were made based on actual observed vortex-blade separation on the video monitor (the video display was calibrated prior to the start of data runs). The position readings were noted for later duplication during the pressure data runs. The parallelism of the BVI was checked.

For the pressure data runs, the tape was removed from the transducers and each of the rotor and tunnel conditions were repeated while the vortex generator was positioned at the previously determined values. At each condition both blade pressure data and acoustic data were recorded. At some of the test conditions, the microphone traverse was moved to several streamwise positions to map out the acoustic field. Due to time constraints this could not be done for every test point.

This process was repeated for each of several vortex generator angle of attack settings. A summary of the test matrix is given in Table 1.

Data acquisition

Three data systems were used during this test. The Standard Wind Tunnel System (SWTS) recorded steady wind tunnel and rotor parameters.

A 32-channel, 16-bit digital data acquisition system acquired the 60 channels of blade pressure data in two sets. One transducer was duplicated between the two sets to check repeatability. The remaining channels were used to record two of

the microphones. The incoming data were anti-alias filtered at 10 kHz. Individual channel gains were recorded as part of the data set. Thirty-two revolutions of data were recorded. Daily calibrations of the pressure transducers were performed by fitting a plexiglass tube over each blade, reducing the pressure inside the sealed chamber several psi, and recording the output voltage change from atmospheric and the gauge pressure.

Acoustic data were digitized on a Macintosh-based, four-channel, 12-bit data system, in three sets, with some microphones duplicated between sets to verify consistency. The ALDAS data acquisition software (Ref. 12) was used for data acquisition and reduction. One blade pressure transducer was also recorded on this system. All incoming data were anti-alias filtered at 10 kHz. Individual channel gains could be set independently to maximize signal-to-noise ratio. Thirty revolutions of data were digitized. (Macintosh system memory was insufficient to digitize 32 revolutions.) In addition to this Macintosh-based system, 30 seconds of data were recorded on a digital PCM recorder for archival purposes. Daily calibrations of the microphones were performed using a pistonphone.

The data acquisition on all data systems was triggered on the 1/rev synch signal, while the sampling clock was controlled by the 1024/rev TTL signal provided by the shaft encoder.

Data processing

Blade pressure data

The nominal data set consisted of pressure data from 32 rotor revolutions. These data were calibrated using the daily pressure calibrations described above. The 32 revolutions of data were ensemble averaged using the rotor 1/rev. Since the data were highly repeatable there was no degradation by the averaging process.

Acoustic data

The acoustic data were processed using the ALDAS program (Ref. 12). The data underwent a preliminary review to determine signal-to-noise ratio relative to background noise and to check for repeatability. Background noise arises from the wind tunnel fan drive, most notably as well-defined harmonics at the lower frequencies, from the flow of air over the test hardware, and from the "self-noise" arising from the air flow over the microphones. Figure 7 illustrates the generally high signal-to-noise (S/N) ratio of the data relative to background noise. The signal levels at all frequencies of interest, except a few isolated values, are well above the background noise levels. Several cases of inadequate S/N for weak BVI were identified for (1) large vortex-blade separation distances and high tunnel speed, and (2) low tip Mach number, even at low tunnel speed. With these exceptions noted, no attempt was made to subtract background noise components from the data.

The repeatability of the data was checked using a limited number of duplicate points. Excellent repeatability was observed (fig. 8) for similar operating conditions during different runs.

Filtering:

Figure 9 is a comparison of typical BVI data with data at the same rotor and wind tunnel operating conditions but with the vortex generator fully retracted (approximately 0.75 rotor blade chord below the rotor), so that BVI effects should be minimal. The residual signal is believed to be due to thickness and loading effects unrelated to the vortex. The figure indicates that the acoustic effect of BVI begins to manifests itself at a frequency of approximately the sixth blade passage harmonic. In addition, as mentioned in the "Wind Tunnel Installation" section above, frequencies below approximately 250 Hz are known to be susceptible to contamination by wall reflections. Therefore, several methods of digitally filtering the data were tried to emphasize the BVI-related characteristics in the signal over the other noise mechanisms present. Figure 10 is a comparison of unfiltered data with the same data high-pass filtered at 325 Hz to suppress the first five blade passage harmonics. Although some differences are noted, the main features, such as pulse width and peak-to-peak amplitude are essentially unaffected. Therefore, there seems little advantage to be gained by filtering the data for this particular test, and hence, the discussion below is based on unfiltered data.

Final data reduction:

The raw acoustic data (30 revolution record lengths) from each run were converted to engineering units utilizing the pistonphone calibration performed on the day of the run. The calibrated data were further processed in two ways. They were ensemble averaged in the time domain using the 1/rev trigger pulse, resulting in a one-revolution long averaged time history. The high revolution-to-revolution repeatability of the data from this test yielded good results with this averaging method. This is probably the result of the highly controlled nature of the experiment where the vortex was not subject to large random motions as is the usual case.

The power spectrum of the calibrated data were also obtained by averaging the FFT's of 14 two

revolution long records. This yielded a frequency resolution of half the 1/rev frequency, which is sufficient to resolve the low frequency harmonic components of interest.

Results

A detailed discussion will be presented of the unsteady features of blade pressures during the BVI encounter. The dependence of the acoustic field, as well as the corresponding blade surface pressures, on various parameters of BVI will be discussed.

Blade pressures

Figure 11 shows the pressure time histories on the upper and lower surfaces of the rotor blade, for a full revolution, at 0.89R for a hover tip Mach number of 0.7 and advance ratio of 0.2 and operating in a near head-on BVI condition (nominally the vortex is impinging directly on the leading edge of the rotor - determined by the video-strobe smoke visualization). It is seen that the flow environment of this rotor is quite busy, in spite of the near-zero collective pitch. The upper surface of the rotor blade at the 90 deg azimuth position exhibits a weak shock, indicative of supercritical flow. Examination of the data at lower Mach numbers (not shown) reveals that the sharp pressure increase disappears, further evidence that this is indeed a shock. There is also a weak BVI interaction that occurs near this point (ψ=90 deg). (Evidently the external vortex is inducing enough of a blade lift variation for the rotor to have a self generated BVI.) However, the most prominent single feature is the parallel BVI event at an azimuth of 180 degrees. This event is the focus of the following discussion.

Figure 12 shows the time histories of Fig. 11 on a greatly expanded scale (from about 175 to 210 deg). Several propagative and convective events are discernible in these data. When the vortex reaches the blade leading edge the upper surface pressures begin an abrupt increase (with the leading edge having by far the largest pressure variation, this variation decreasing strongly with distance from the leading edge - events with opposite sign occur on the bottom surface). The fact that these particular events occur almost simultaneously from leading to trailing edge is indicative of a very rapid propagative event - downstream from leading to trailing edge - whose propagation speed is the local speed-of-sound plus the local flow velocity. The effect of this first BVI wave appears to be the establishment of a fairly steady pressure level that persists for some duration. The time of persistence is greatest near the leading-edge and appears to be a nearly linear function of distance from the leading edge. During this persistence interval, several occurrences are seen to move downstream at a slower speed that is of the order of the mean flow velocity. For this particular interaction this slower event is most clearly seen on the bottom surface. These are obviously events that are associated with the chordwise passage of the vortex and vortex generated flow features (possibly vortex-induced boundary-layer disturbances). These two occurrences were previously noted in the earlier tests that were conducted in the Army 7- by 10-Foot Wind Tunnel (Refs. 6-8). However, the present data also show an additional propagative event not seen in the 7x10 test. At about the time the previously mentioned convective events approach the trailing edge a new wave appears - propagating upstream from the trailing edge. This wave has a fairly broad width and moves upstream relatively slowly (at the speed of sound minus the convection speed). Undoubtedly this wave is the trailing edge Kutta condition asserting itself either in response to the passing vortex or to the original BVI wave - and propagating that information upstream. This secondary or "Kutta wave" occurs at the same time and has opposite sign on the top and bottom surfaces.(Because the sign is opposite, we believe that this latter wave is primarily a response to the primary wave rather than to the vortex itself. The inviscid effect of a vortex at a sharp edge is an expansion on both sides.) This wave is fairly weak (compared to the initial BVI pulse) and was not seen in previous 7x10 testing due to flow unsteadiness. The ability to observe this wave is indicative of the much cleaner flow quality in the 80x120. Similar upstream waves emanating from the trailing edge were recently observed by Obermeier and Schurmann (Ref. 9) in high-speed interferometric studies conducted in a shock tube.

The effect of the BVI on the chordwise pressure distribution is shown in Fig. 13 for the same BVI event shown in Fig. 12. Figure 13a shows the chordwise pressure distribution at an azimuth of about 176 deg, which is very shortly before the impact of the vortex on the leading edge. At this point the lift is still quite small but beginning to rise rapidly. Figure 13b shows the pressure distribution very near the moment of impact of the vortex center on the leading edge. At this point the lift is a maximum and begins to drop rapidly. Figure 13c shows the pressure distribution only 3 deg later. At this point the lift is zero and dropping. The lift continues to drop until Fig. 13d ; the entire shape of the pressure distribution is distorted resulting in a significant differential pressure in the trailing-edge region. (This trailing edge loading results in a sharp moment pulse and blade "ringing" that was clearly seen in the root torsion strain gages.) This point closely corresponds to the point at which the chordwise moving wave commences. After this point we see the re-establishment of

circulatory lift and the differential pressure reduces, as does the total lift. Figures 13e and f show the evolution of the chordwise pressure distribution as the "Kutta wave" propagates upstream. This last point constitutes the termination of the BVI event. We define the BVI event as that period beginning when the vortex passes the leading edge and ending when the resulting Kutta wave passes the leading edge. These are two easily identifiable events during which time the blade turns about 30 deg of azimuth - or about 3 chords of travel at this radial station.

Directivity

For the directivity study the sound pressure levels at the five far-field microphones were normalized, using a 1/r dependence, to a constant distance to better display the directivity characteristics of the acoustic field. The reference distance for this normalization was arbitrarily chosen to be the distance to Microphone #3 when the microphone traverse was directly to the side of the rotor hub (ψ=270 deg). Figure 14 presents a partial map of the acoustic field around the rotor for a typical BVI condition. The elevation angle ϕ is defined with respect to the rotor plane (positive down) and the azimuth angle ψ is defined with origin at the rotor hub and measured positive clockwise (in the direction of rotation) from the downstream direction. The main point is that the acoustic directivity related to BVI occurring at ψ = 180 deg has a wide lobe directly to the side and below the rotor. The maximum peak acoustic pressure level is observed at ψ=270 deg and ϕ=47 deg, although this is not a very sharply defined maximum. It's unclear whether the actual maximum has actually been reached at this elevation angle. Possibly, it may be at an even larger angle. Similar directivity patterns were obtained for other operating conditions. In some cases there were indications that the peak of the directivity lobe was actually somewhat upstream of the ψ=270 deg angle. We could not resolve the directivity to any better extent because time constraints did not allow a more extensive exploration of the sound field.

The presence of two secondary pulses is evident in Fig. 14. The increase in the time delay between these secondary pulses and the main pulse with microphone height clearly indicates that these are reflections of the BVI pulse, most likely by localized hard areas on the wind tunnel floor. They do not seem to contaminate the main BVI pulse.

For the analyses presented below, Microphone #3 at ψ=270 deg and ϕ=37 deg was chosen as representative of the main features of the acoustic field.

Vortex proximity

At each rotor operating condition the vortex generator was traversed vertically to place the vortex at several desired separation distances during the BVI encounter. Figure 15 is a plot of the blade leading edge (0.020 chord) pressure near the vicinity of the BVI encounter as a function of vortex proximity (in rotor blade chords). Note that the maximum blade pressure peak occurs when the vortex is 0.125-chord above the blade, rather than for direct impact. This, we think, is due to our inability to accurately judge small changes in vortex position and indicates the extreme sensitivity of BVI aerodynamics to vortex proximity. Although the vortex placement was set visually - with the flow visualization clearly defining the blade and the vortex core - it was not possible in the time available to set the miss distance with absolute confidence due to the extreme sensitivity of the interaction to miss distance.

Figure 16 is the corresponding Mic #3 waveform. The peak amplitude is observed to occur when the vortex is between 0.125-chord and 0.25-chord above the blade in agreement with the blade pressure data.

Figures 15 and 16 demonstrate the sensitivity of both BVI aerodynamics and acoustics to small variations in vortex proximity to the blade during encounter. An increase in vortex proximity of one quarter of a blade chord produces a 35 percent reduction in peak surface pressure as well as a 35 percent reduction in peak acoustic pressure.

Vortex sense and strength

Figures 17a and 17b illustrate the influence of vortex sense and strength (as determined by the vortex generator angle of incidence) on the blade surface pressures and the acoustic field, respectively. These cases are for nominally head-on interaction. The bottom surface pressures nearest to the leading edge are chosen to be indicative of the effect of the vortex generator angle on the rotor near-field. A simple way to quantify this effect on surface pressure is to compare the BVI pressure rise, defined on Fig. 17a, between the pressure peak (the point at which the vortex impinges on the leading edge) and the subsequent relatively constant pressure level. (In Fig. 17a the pressure levels and BVI locations are shifted in order to more clearly show the differences between the plots.) The pressure difference for an incidence angle of 6 deg is about 60 percent of that for the 12 deg case, which is somewhat higher than expected, but not a total surprise because of the previously mentioned sensitivity to vortex location. At 6 deg the peak far-field pressure at the location of Microphone #3 is about 75 percent of that for 12

deg. This is somewhat higher than we expect based on the blade surface pressures. Reversing the sign of the vortex results in the reversal of the BVI pulse, both on the blade and at the microphones. The acoustic pressure level for -12 deg is about 40 percent higher than for +12 percent. The surface pressure difference is similarly higher, in good agreement with the microphone data. This difference in magnitude is larger than would be expected from errors in vortex location and may be due to an alignment error in the vortex generator incidence angle.

Rotor tip Mach number

Figures 18 and 19 show the influence of rotor tip Mach number. The horizontal axis in the sound pressure plot has not been scaled to account for RPM changes. As expected, tip Mach number is an important parameter determining the acoustic pressure amplitude. A reduction in tip Mach number from 0.7 to 0.6 results in a 40 percent reduction in peak sound pressure amplitude. The dominant mechanism for the strong Mach number dependence is revealed by examining the effect of tip Mach number on blade pressures (expressed in coefficient form). Figure 18 indicates that there is actually a small Mach number dependence over a large speed range. The implication is that the dependence of acoustic pressure is primarily due to differences in Doppler factor and the local dynamic pressure.

Concluding Remarks

A parametric study of parallel blade-vortex interaction aerodynamics and acoustics was carried out using a small-scale pressure-instrumented rotor interacting with a vortex generated independently of the rotor. The test was conducted in the NASA Ames 80- by 120-Foot Wind Tunnel. This approach of operating a small model in an extraordinarily large tunnel permitted the acquisition of high quality acoustic data on this high frequency interaction noise mechanism. It appears that for acoustic purposes the testing of small models is a very appropriate use of a large wind tunnel.

Although this basic set-up had been used previously, this was the first test wherein it was possible to obtain both blade loading data and the accompanying acoustic data. This test was also more revealing than the prior small tunnel tests because the superior flow in the 80x120 permitted the resolution of significant flow features that had previously been masked by flow unsteadiness. The primary BVI leading-edge pressure pulse is a large amplitude event that was clearly seen previously. The present test also revealed the presence of previously seen convective disturbances traveling rearward from the leading edge - this is undoubtedly the vortex or it's remnants and possibly some boundary layer eruptions. However, in this test it was discovered that there is actually a second much weaker acoustic wave generated at the trailing edge. This wave has opposite sign on the top and bottom surfaces and it has the effect of terminating a distinct non-circulatory lift which occurs following the primary BVI. Therefore, this secondary wave, while probably not of great acoustic significance, does represent an important aerodynamic flow feature. The ability to predict this wave is probably a good accuracy test for a CFD method.

The BVI process displays a number of interesting features, of which the initial leading-edge pressure jump is by far the most prominent - and the most important for acoustic propagation. A close correlation was found between the acoustic and blade pressure data. That is, although the BVI interactions sometimes were not entirely what was expected - probably due to small errors in vortex placement or angle settings - it was found that surface pressure features were always closely reflected in the microphone data.

The most sensitive parameter governing the BVI was the blade-vortex proximity. For close interactions a variation of 0.25 chords in miss distance can change the BVI strength by a factor of two. We assume that such sensitivity would only increase for the smaller core size typical of operational rotors. (The present core size was large - of the order of 0.5 blade chords).

The BVI acoustic signal was also very sensitive to tip Mach number. However, this sensitivity was mainly due to changes in the local blade dynamic pressure and in the Doppler factor. The sensitivity of the local blade flow (judging from the leading edge transducers) to tip Mach number seemed remarkably small (especially in view of the previously mentioned difficulty in consistently locating the vortex.)

In summary the present test set-up worked very well. It produced data that will be invaluable for the validation of CFD flow and acoustic codes and a necessary code development step prior to the modeling of full rotor-wake flow and acoustics.

Acknowledgments

The authors wish to acknowledge the assistance of Steve Dunagan, Scott Harris, Jon Lautenschlager, and Megan McCluer in the performance of this test.

References

1. George, A.R. and Chang, S.B., "Noise Due to Transonic Blade-Vortex Interactions," American Helicopter Society 39th Annual Forum, St. Louis, MO, May 1983.

2. Brentner, K.S., "Prediction of Helicopter Rotor Discrete Frequency Noise," NASA TM 87721, October 1986.

3. Gallman, J.M., "The Validation and Application of a Rotor Acoustic Prediction Computer Program," Army Science Conference, Durham, NC, June, 1990.

4. Xue, Y. and Lyrintzis, A.S., "The Use of a Rotating Kirchoff Formulation for 3-D Transonic BVI Far-Field Noise," American Helicopter Society 49th Annual Forum, St. Louis, MO, May, 1993.

5. Baeder, J.D., "The Computation and Analysis of Acoustic Waves In Transonic Airfoil-Vortex Interactions," Ph. D. Thesis, Stanford University, Sept. 1989.

6. Caradonna, F.X., Laub, G.H., and Tung, C., "An Experimental Investigation of the Parallel Blade-Vortex Interaction," 10th European Rotorcraft Forum, The Hague, Netherlands, Sept. 1984.

7. Caradonna, F.X., Lautenschlager, J.L., and Silva, M.J., "An Experimental Study of Rotor-Vortex Interactions," AIAA Paper No. 88-0045, AIAA 26th Aerospace Sciences Meeting, Reno, NV, Jan., 1988.

8. Caradonna, F.X., Strawn, R.C., Bridgeman, J.O., "An Experimental and Computational Study of Rotor-Vortex Interactions," 14th European Rotorcraft Forum, Milano, Italy, Sept., 1988.

9. Obermeier, F. and Schurmann, O., "Experimental Investigation on 2D Blade-Vortex-Interaction Noise, " AIAA Paper No.93-4334, 15th AIAA Aeroacoustics Conference, Long Beach, CA, Oct. 25-27, 1993.

10. Straus, J., Renzoni, P., and Mayle, R.E., "Airfoil Pressure Measurements During a Blade Vortex Interaction and a Comparison with Theory," *AIAA Journal*, Vol. 28, No.2, Feb. 1990.

11. McAlister, K.W. and Takahashi, R.K., "NACA 0015 Wing Pressure and Trailing Vortex Measurements," NASA Technical Paper 3151, November 1991.

12. Watts, M.E., "ALDAS User's Manual," NASA TM 102831, April 1991.

TABLE 1 - TEST MATRIX

M_{tip}	μ	α_v
0.7	0.2	-12°, +12°, +6°
0.6	0.1	-12°, +12°
	0.15	-12°, +12°
	0.2	-12°, +12°, +6°
0.5	0.2	+12°
0.4	0.2	-12°, +12°
0.25	0.2	-12°, +12°

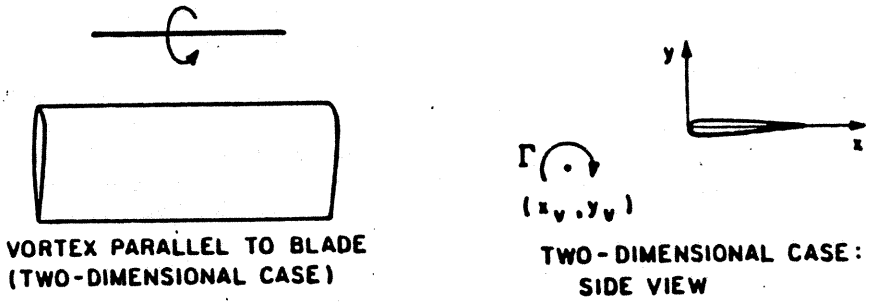

Figure 1. Analytical model of parallel blade-vortex interaction

Figure 2. BVI experiment in the NASA Ames 80- by 120-Foot Wind Tunnel

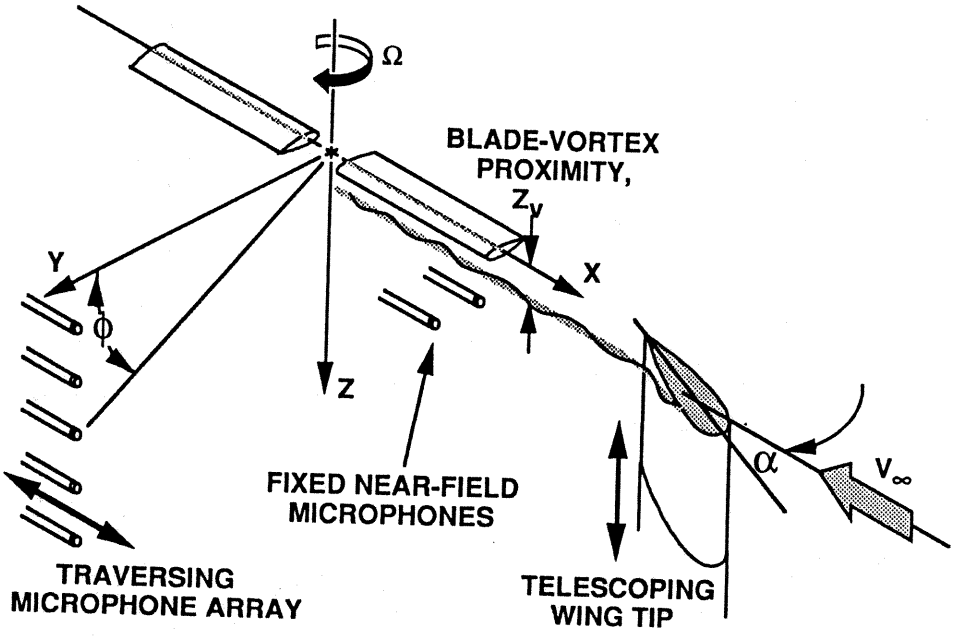

Figure 3. Sketch of BVI test set-up and definition of parameters

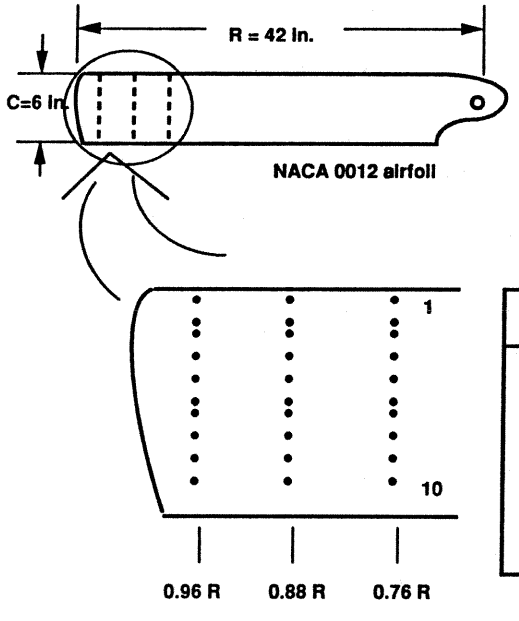

Transducer	Chordwise position
1	0.02
2	0.11
3	0.20
4	0.31
5	0.40
6	0.48
7	0.56
8	0.64
9	0.72
10	0.83

Figure 4. Blade pressure transducer locations (not to scale).
Identical locations for upper and lower surfaces.

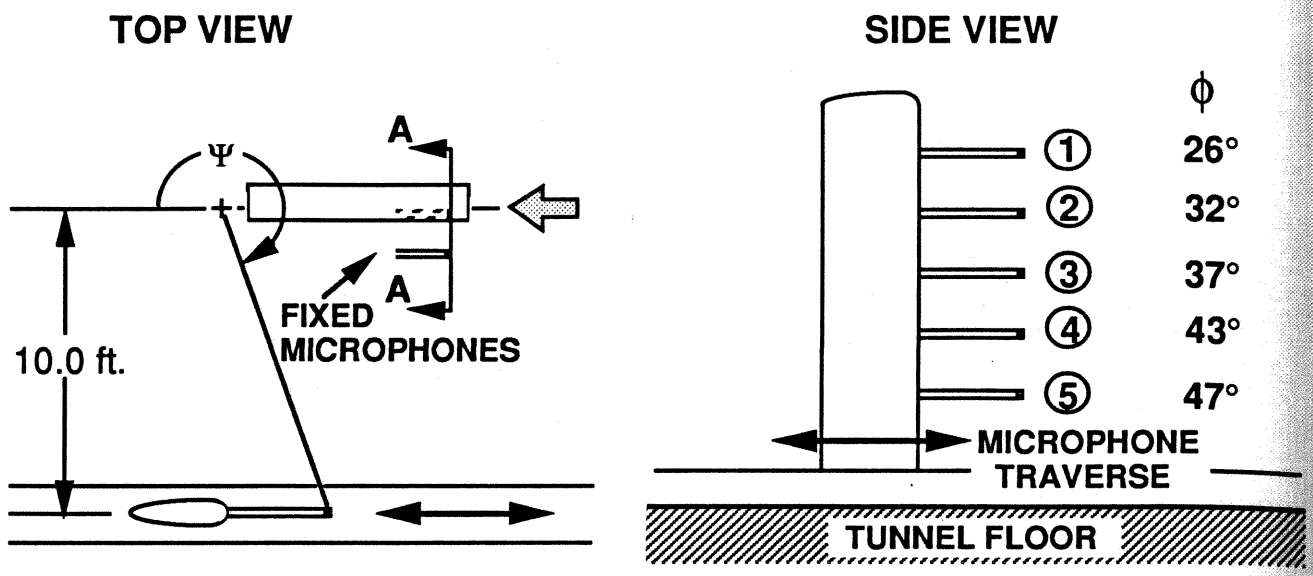

Figure 5. Far field microphone positions (not to scale). Elevation angles are relative to the rotor plane.

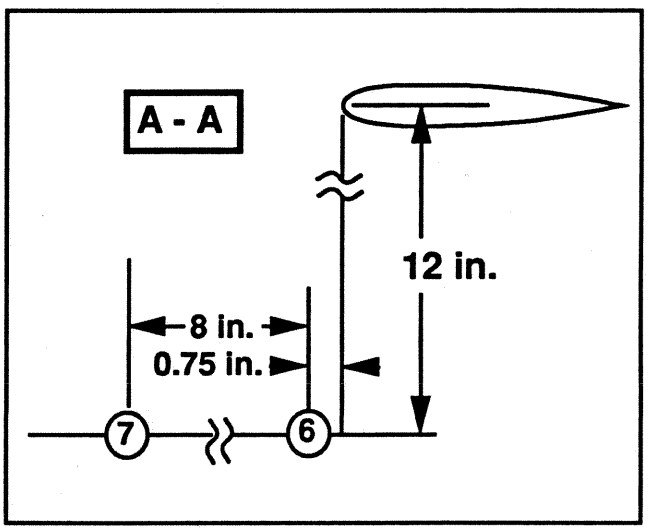

Figure 6. Near-field microphone positions (not to scale)

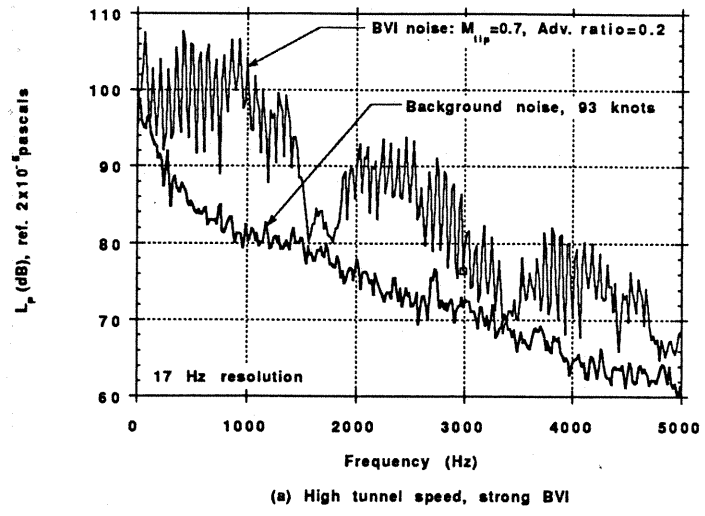

(a) High tunnel speed, strong BVI

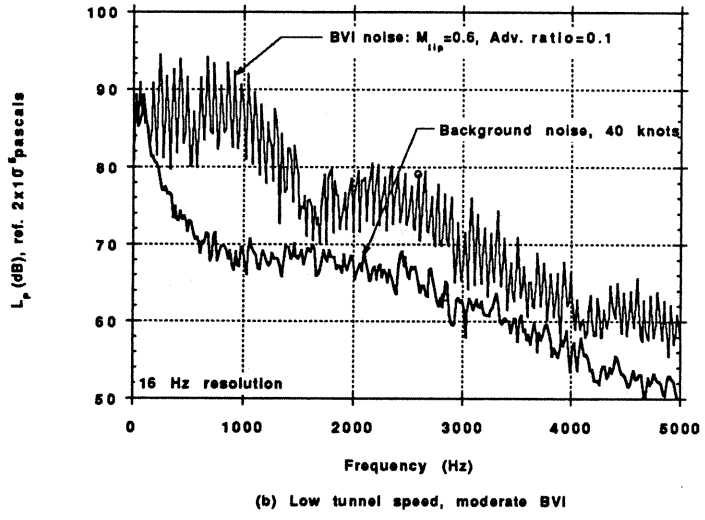

(b) Low tunnel speed, moderate BVI

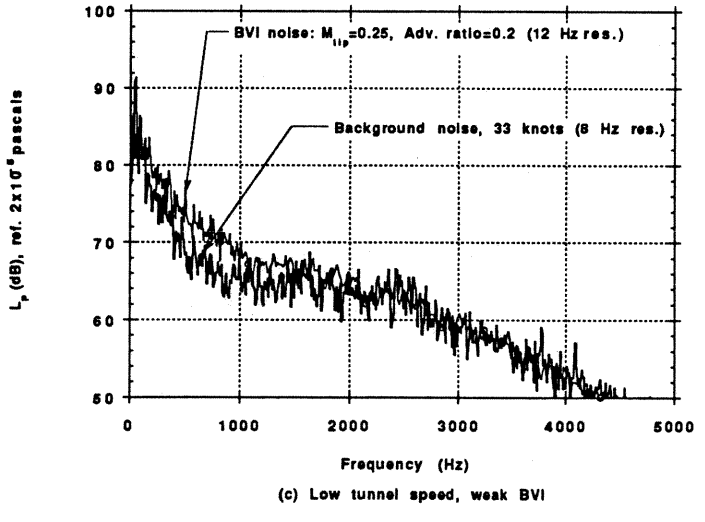

(c) Low tunnel speed, weak BVI

Figure 7. Comparison of BVI noise to background noise. Cases (a) and (b) show good signal-to-noise, case (c) indicates unsatisfactory signal-to-noise.

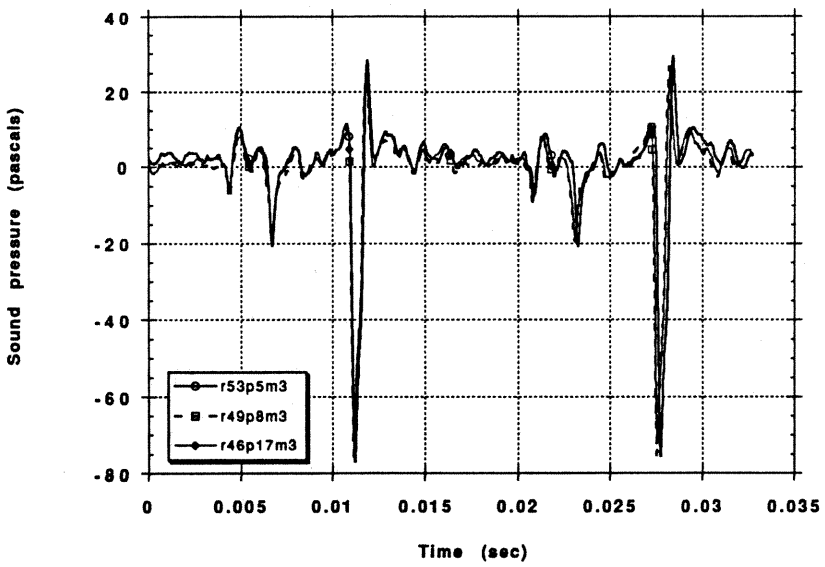

Figure 8. Data repeatability. All three data sets: M_{tip}=0.6, Adv. ratio = 0.2

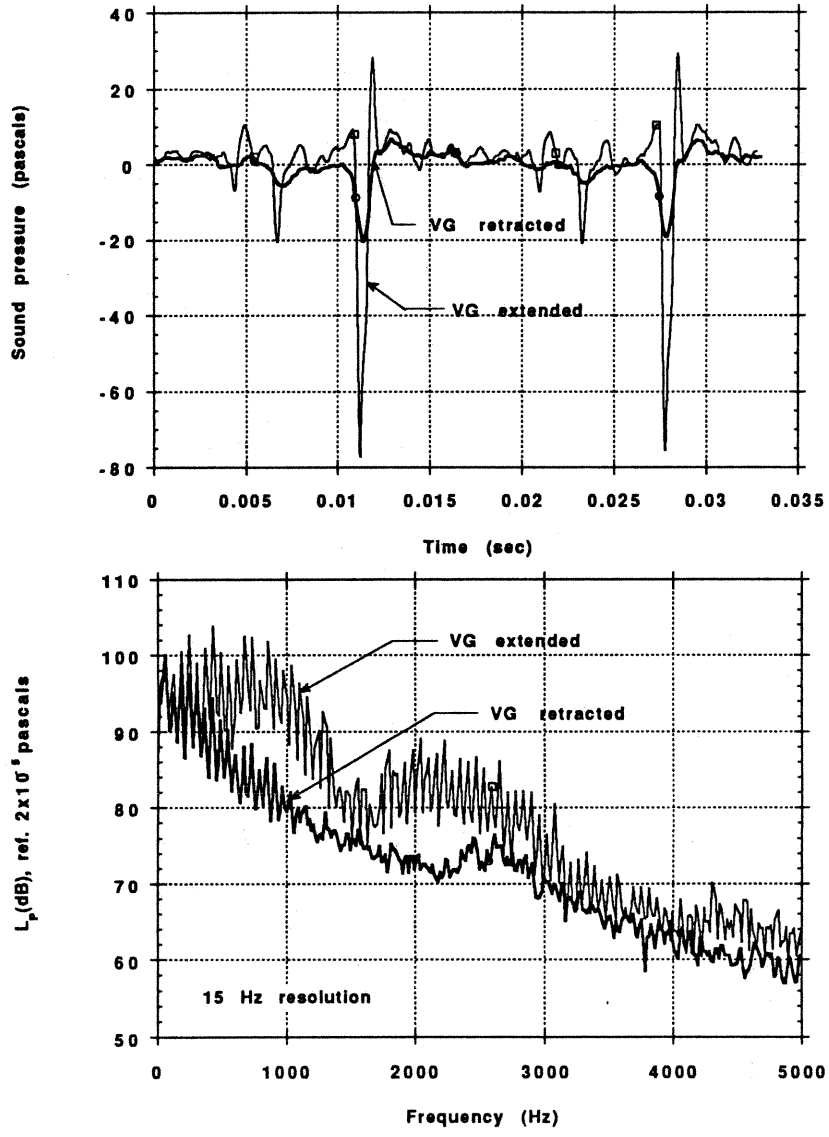

Figure 9. Effect on rotor noise of the presence of the vortex.
M_{tip}=0.6, Adv. ratio = 0.2, Mic #3 (ψ = 270°, ϕ = 37°)

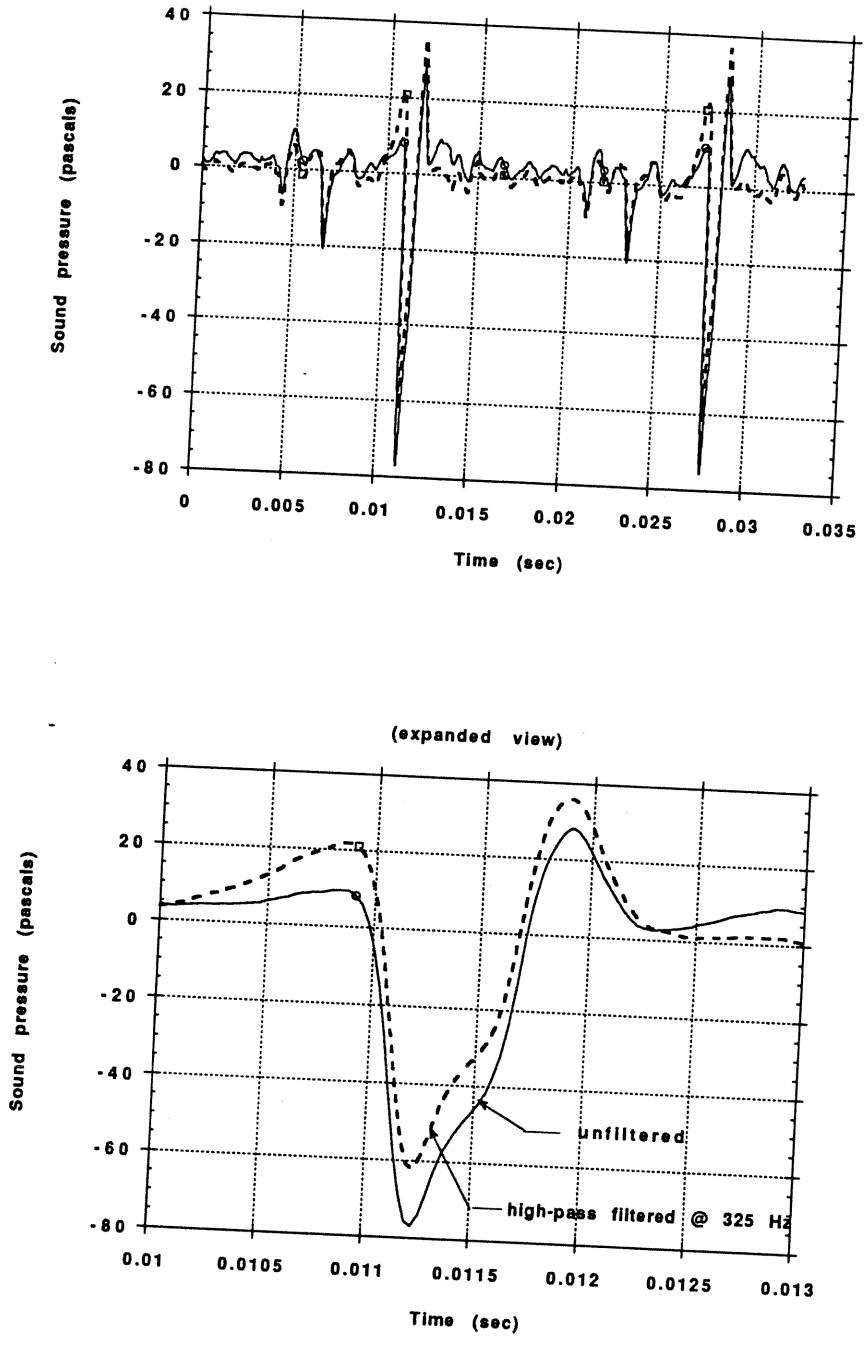

Figure 10. Effect of filtering. $M_{tip} = 0.6$, Adv. ratio = 0.2

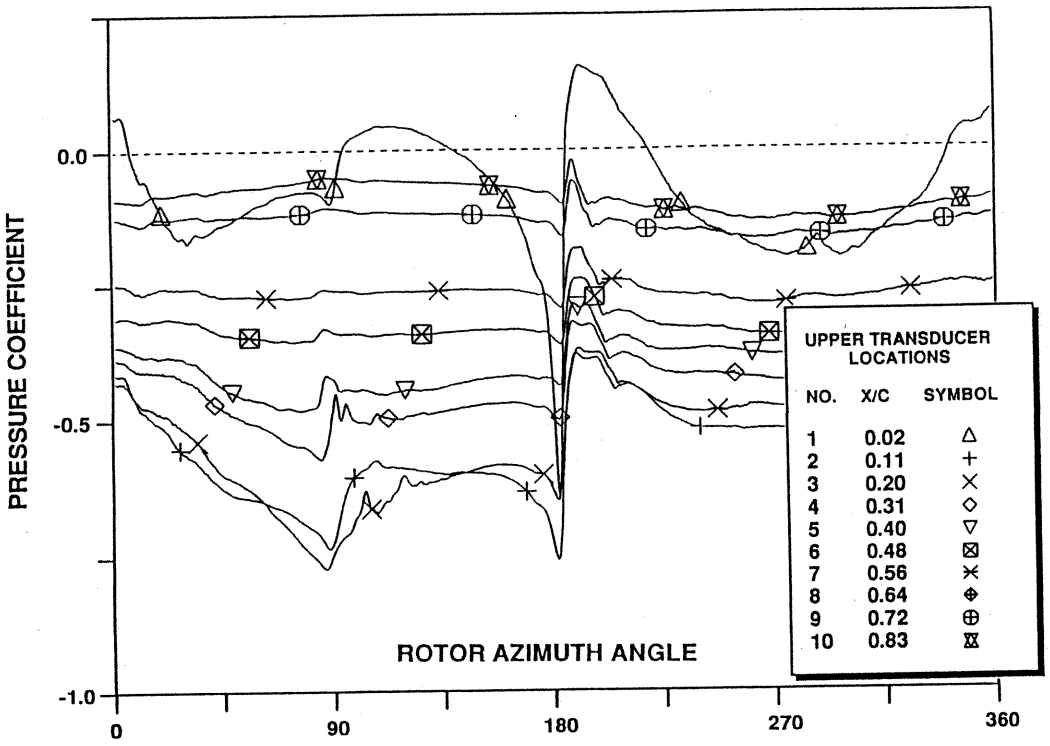

(a) Upper surface

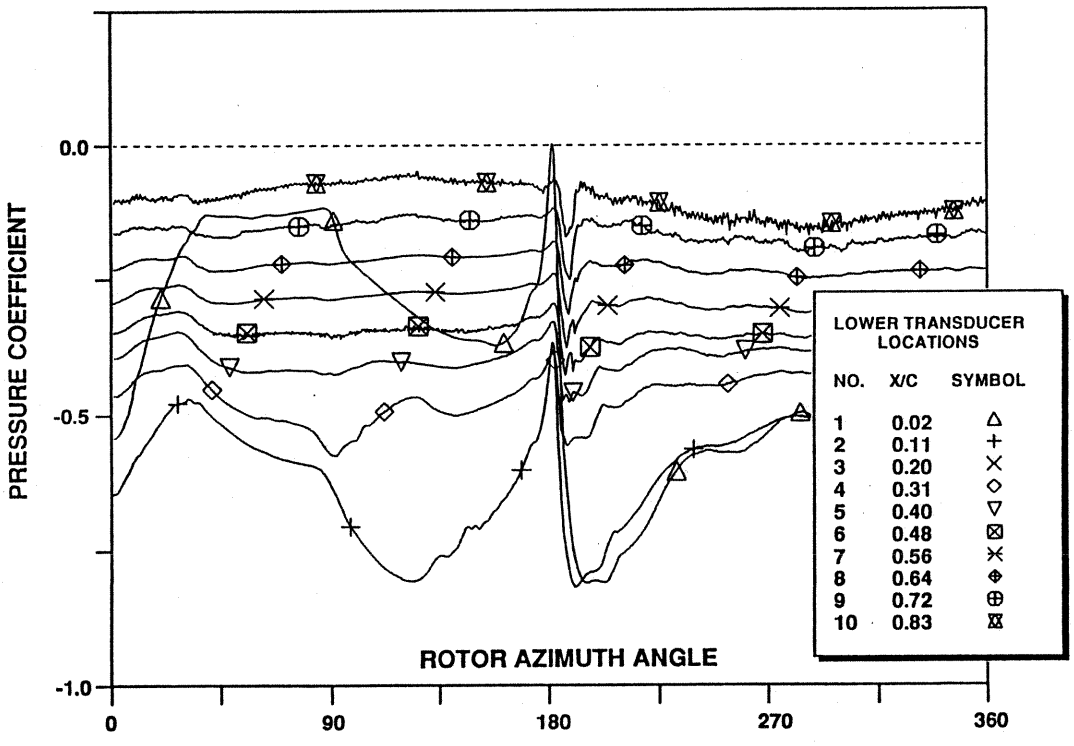

(b) Lower surface

Figure 11. Blade pressure variations induced by parallel BVI. M_{tip}= 0.70, μ = 0.2, α_v= +12°, z_v= 0.

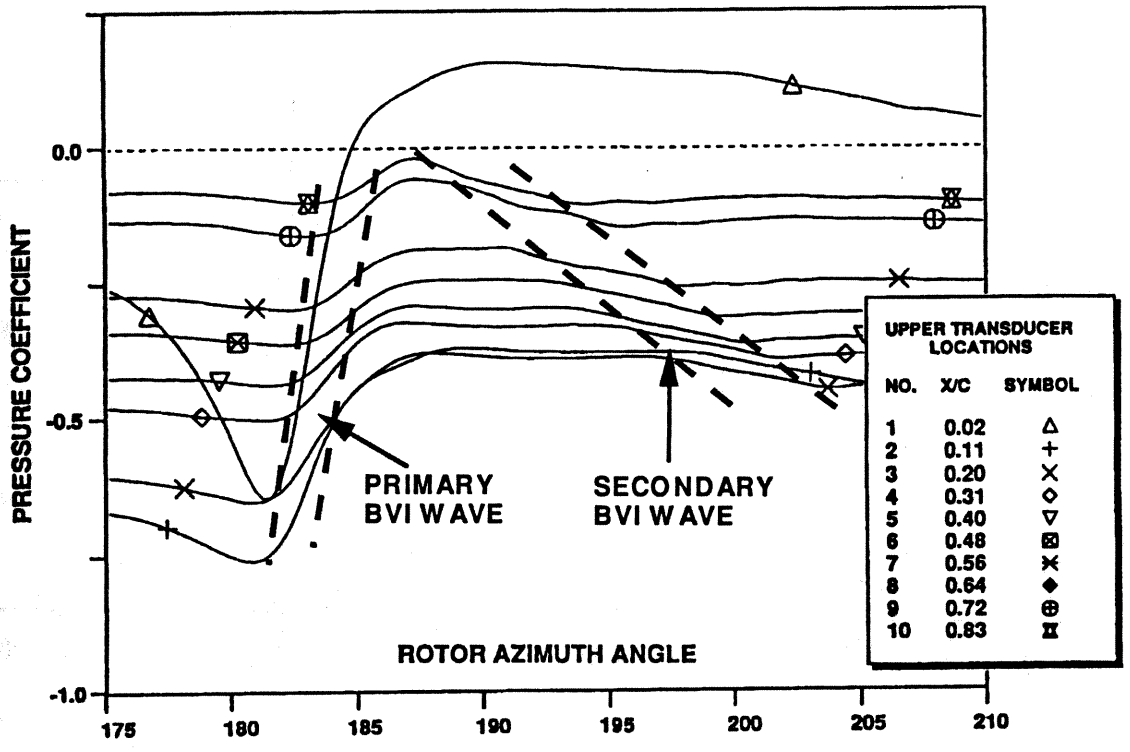

(a) Upper surface

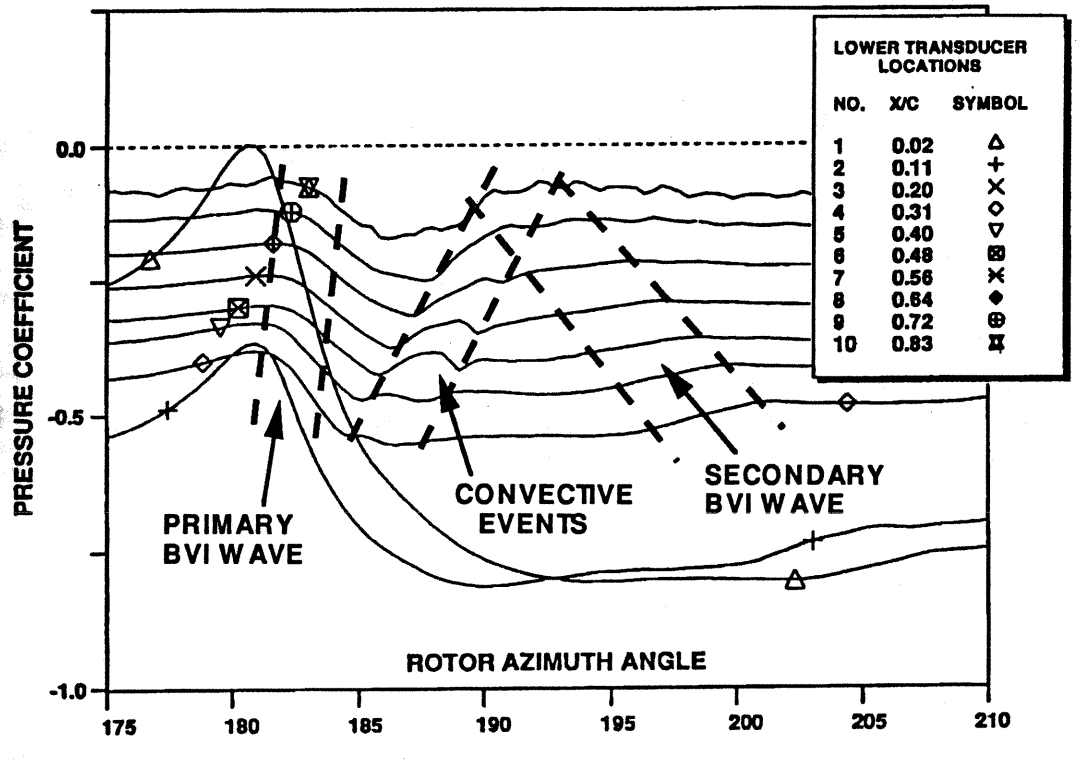

(b) Lower surface

Figure 12. Blade pressure variations induced by parallel BVI. Expanded azimuth scale. M_{tip}= 0.70, μ = 0.2, α_v= +12°, z_v= 0.

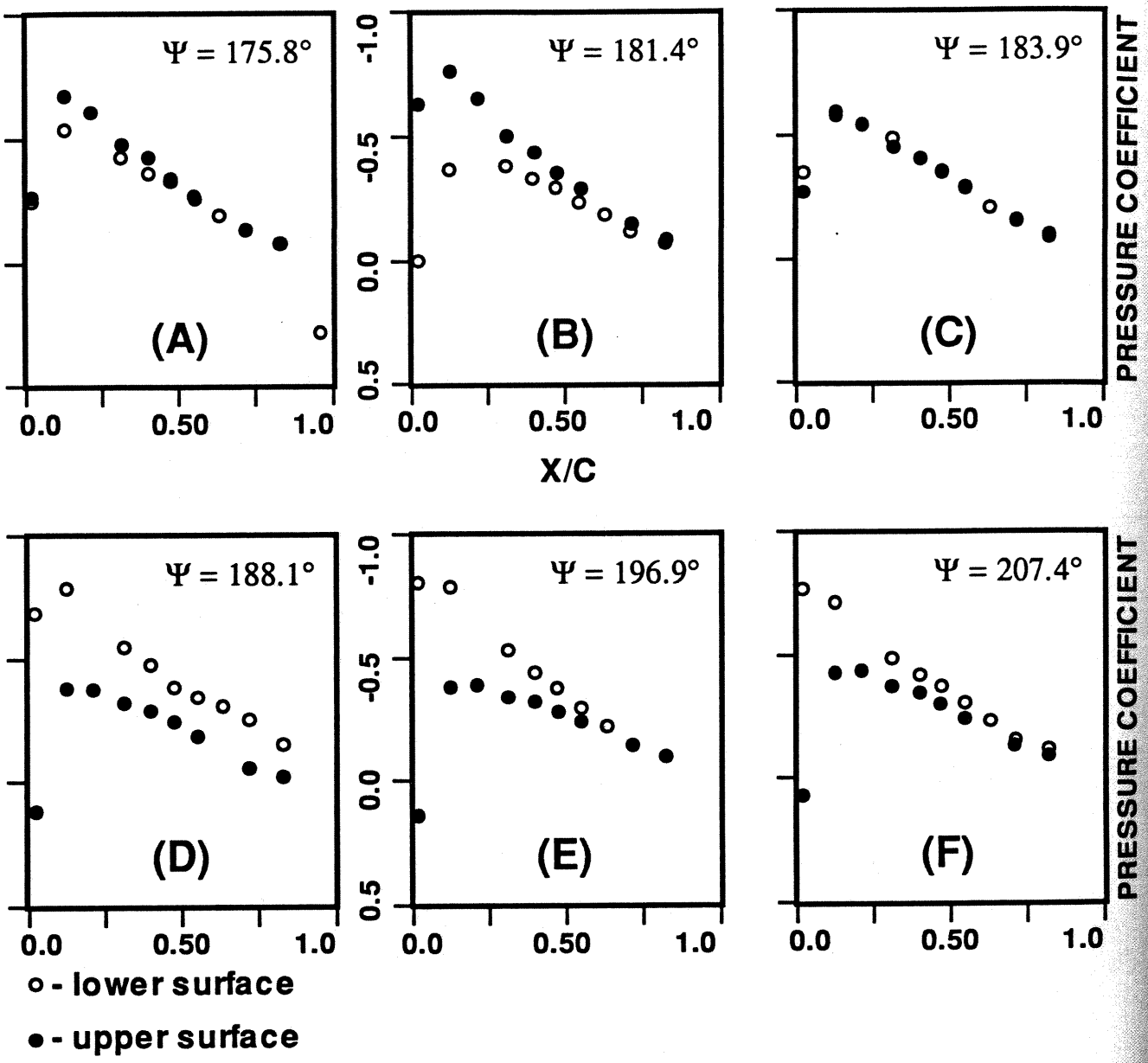

Figure 13. The Effect of a Parallel BVI on the Rotor Chordwise Pressure Distribution.
Mtip = 0.70, μ = 0.2, r/R = 0.89, α = +12°

$\psi = 252°$ $M_{tip} = 0.6, \mu = 0.2, \alpha_v = +12°, z_v = 0.$ $\psi = 261°$

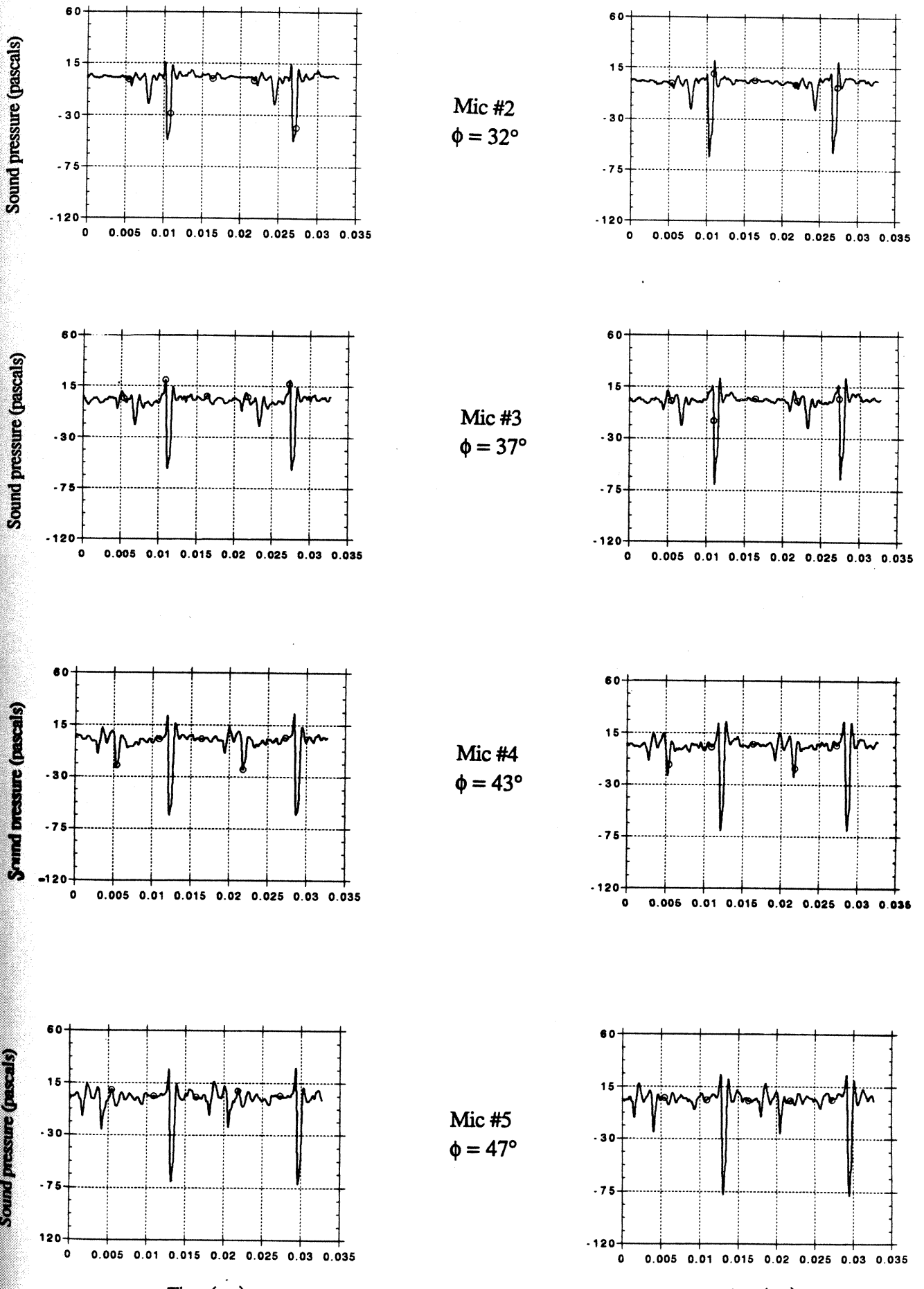

Figure 14. BVI directivity.

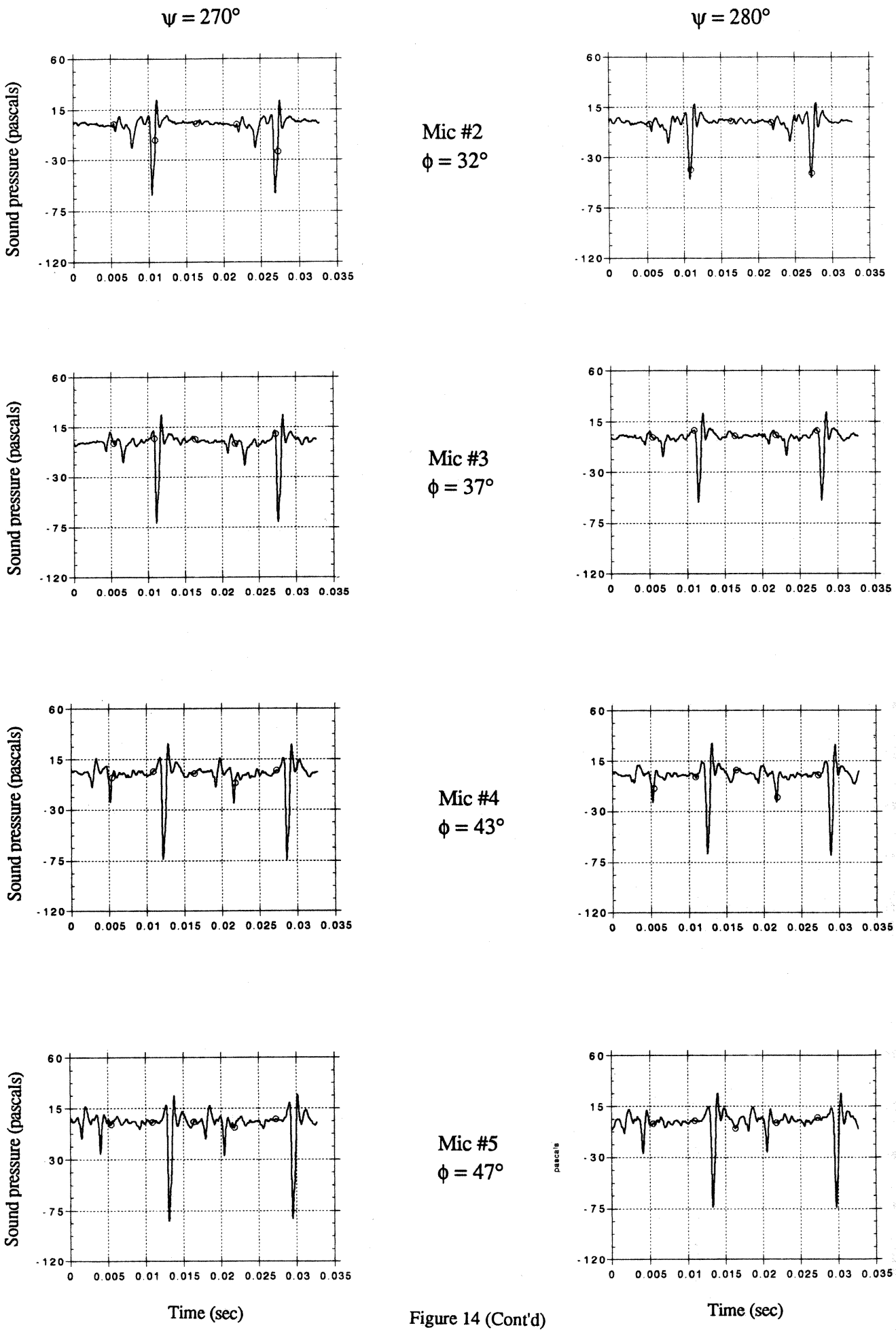

Figure 14 (Cont'd)

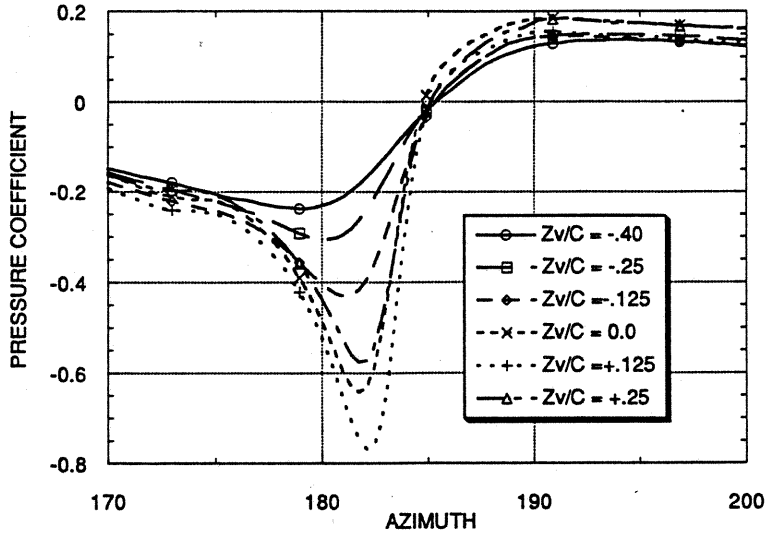

Figure 15. Effect of vortex proximity on blade leading edge pressure coefficient. M_{tip}= 0.7, μ = 0.2, α_v= +12°, 0.89R.

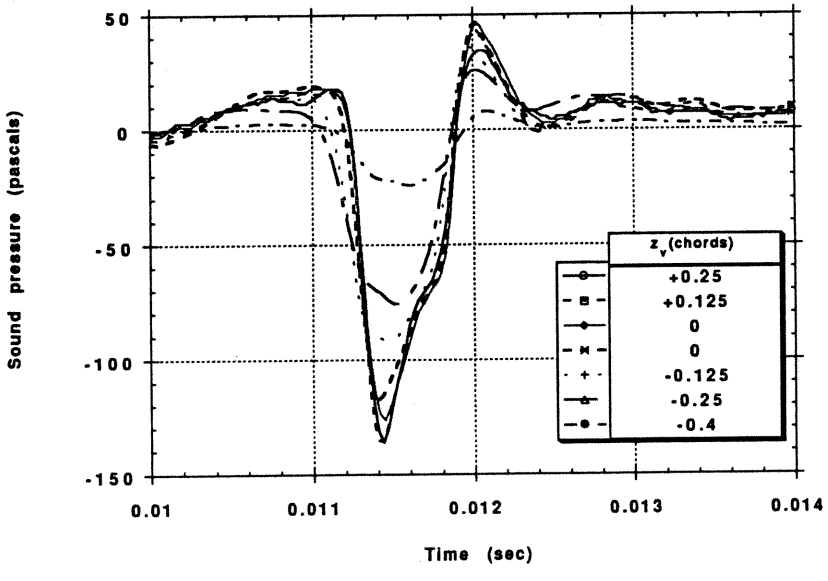

Figure 16. Effect of vortex proximity on far-field BVI sound pressure. M_{tip} = 0.7, μ=0.2, α_v=+12°, Mic #3 (ψ = 270°, ϕ = 37°)

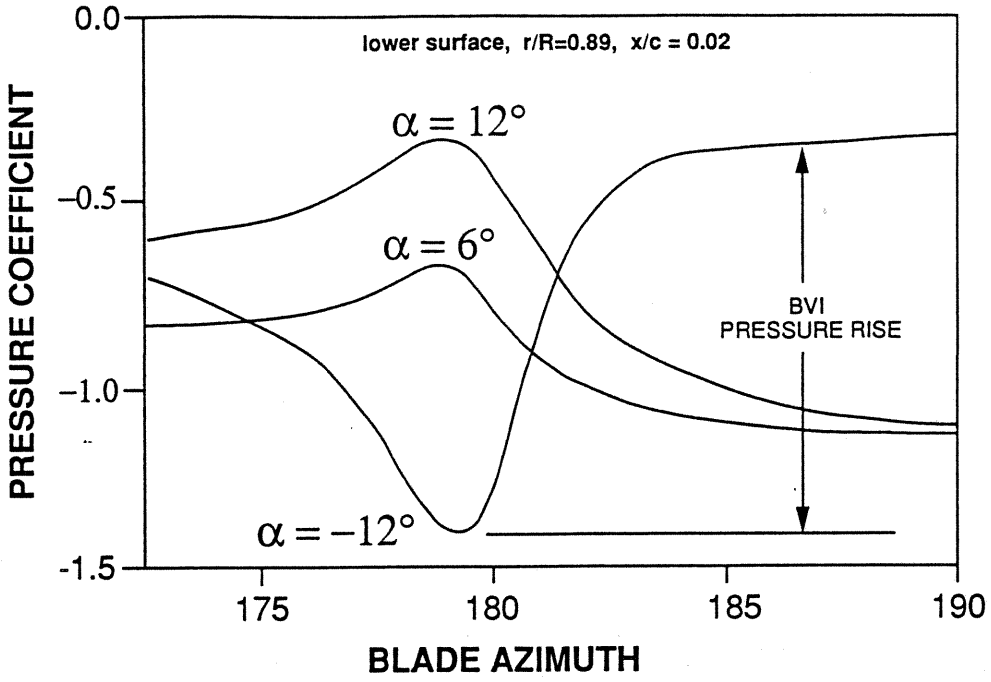

Figure 17(a). The effect of vortex strength and sense on BVI surface pressure variations.
$M_{tip} = 0.7, \mu = 0.2, Z_v/c = 0.0$

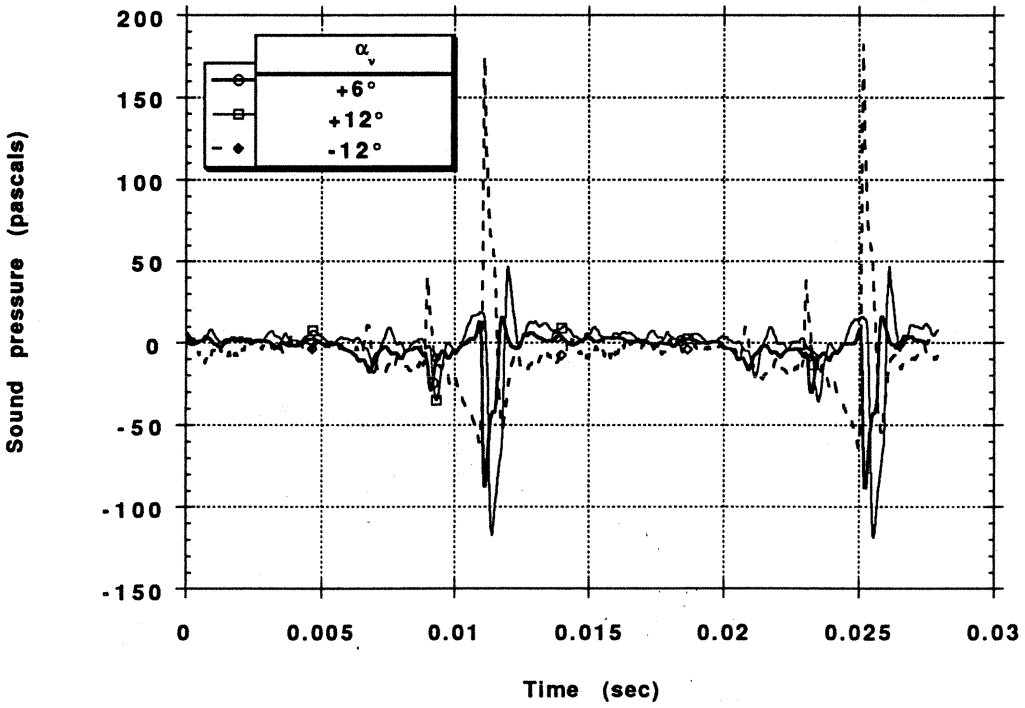

Figure 17(b). Effect of vortex strength and sense on far-field BVI sound pressure.
$M_{tip} = 0.7, \mu = 0.2, z_v = 0$ (direct impact), Mic #3 ($\psi = 270°, \phi = 37°$)

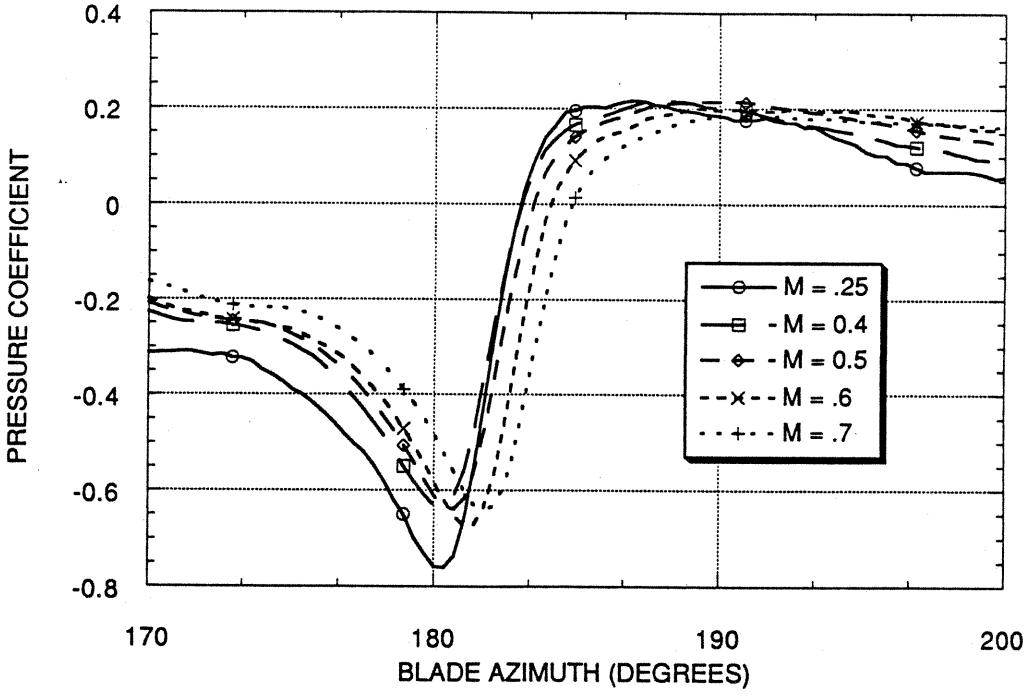

Figure 18. The effect of tip Mach number on leading edge pressure variation. Advance ratio = 0.2, Z_v/c = 0.0, upper surface, x/c = 0.02, r/R = 0.89 α = +12°

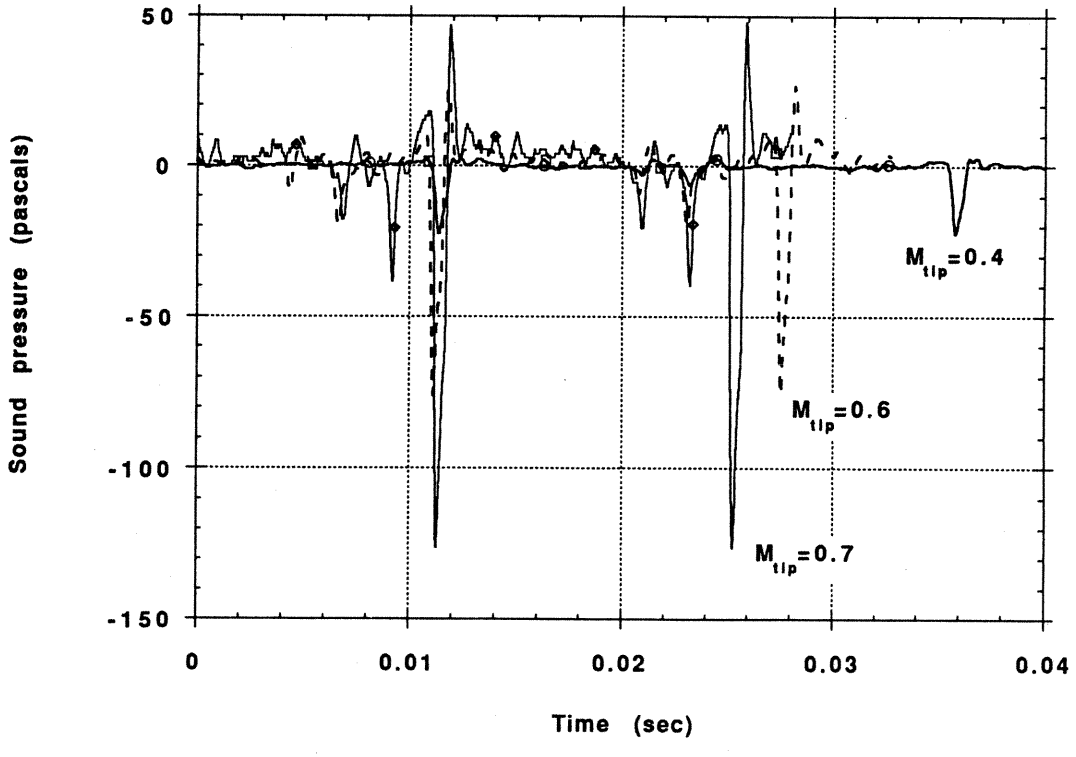

Figure 19. Effect of rotor tip Mach number on far-field BVI sound pressure. μ = 0.2, α_v = +12°, z_v = 0 (direct impact), Mic #3 (ψ = 270°, ϕ = 37°)